Research Square

Preprints are preliminary reports that have not undergone peer review.
They should not be considered conclusive, used to inform clinical practice,
or referenced by the media as validated information.

A Novel Dual Particle Filter - Based Approach for Joint Online Estimation of State of Charge and State of Health in Lithium-ion Battery Packs

Nana Zhou
Shandong Xiehe University
Lianfeng Lai
Ningde Normal University
Zhihui Deng
Ningde Normal University
Fengjun Zhou
Shandong Xiehe University
Bing Lu
Beijing Institute of Technology
Weiwei Huo
Beijing Information Science & Technology University
Yonghong Xu
xyhcomeonljx@126.com

Beijing Information Science & Technology University

Article

Keywords: battery pack, state of charge, health state, joint estimation, dual particle filter

Posted Date: April 29th, 2026

DOI: https://doi.org/10.21203/rs.3.rs-9342981/v1

License: This work is licensed under a Creative Commons Attribution 4.0 International License.
Read Full License

Additional Declarations: No competing interests reported.

Title: A Novel Dual Particle Filter - Based Approach for Joint Online Estimation of State of Charge and State of Health in Lithium-ion Battery Packs

First author: Nana Zhou

Order of authors: Nana Zhou[a], Lianfeng Lai [b*], Zhihui Deng [b], Fengjun Zhou[a], Bing Lu[c*], Weiwei Huo[d], Yonghong Xu[d*]

Authors' institution:

[a] Shandong Xiehe University

[b] Ningde Normal University

[c] Beijing Institute of Technology

[d] Beijing Information Science and Technology University

***Corresponding authors:** Lianfeng Lai (lailianfeng2020@163.com), Bing Lu (lubing@bitzh.edu.cn), and Yonghong Xu (xyhcomeonljx@126.com)

A Novel Dual Particle Filter - Based Approach for Joint Online Estimation of State of Charge and State of Health in Lithium-ion Battery Packs

Nana Zhou[a], Lianfeng Lai [b*], Zhihui Deng [b], Fengjun Zhou[a], Bing Lu[c*], Weiwei Huo[d], Yonghong Xu[d*]

[a] School of Computer Science, Shandong Xiehe University, Jinan 250109, Shandong, China

[b] College of Mechanical and Electrical Engineering, Ningde Normal University, Ningde 352000, China

[c] Beijing Institute of Technology, Zhuhai, 519085, PR China

[d] School of Electrical and Mechanical Engineering, Beijing Information Science and Technology University, Beijing 100192, China

Abstract

This study establishes equivalent circuit models for battery packs with four distinct connection methods: series connection, parallel connection, series-parallel connection, and parallel-series connection. A dual particle filter (DPF) algorithm is employed to jointly estimate the state of charge (SOC) and state of health, with the aim of exploring the performance differences among them. Given that the initial value has a substantial impact on the estimation accuracy of the DPF algorithm, the particle swarm optimization algorithm (PSO) is utilized to optimize the initial value of the DPF, thereby enhancing its estimation performance. To validate the accuracy of the SOC estimation, dynamic stress test (DST) working conditions are adopted. The performance of the DPF algorithm is compared with that of the dual extended Kalman filter (DEKF) and extended Kalman filter (EKF) algorithms. The results unequivocally demonstrate that the DPF algorithm outperforms the DEKF and EKF algorithms in terms of SOC estimation accuracy. Specifically, for the four different battery packs, the root mean square error and mean absolute error) of the SOC estimation using the DPF algorithm are all below 2%. This indicates that the DPF algorithm exhibits high estimation

accuracy and robustness, providing a valuable reference for lithium-ion battery packs.

Keywords: battery pack, state of charge, health state, joint estimation, dual particle filter

1. Introduction

The development of modern civilization is inseparable from fossil fuels, however, fossil energy also brings a series of challenges [1]. Fossil energy not only cause environmental pollution but are also being steadily depleted, with impacts that are worsening over time [2]. Lithium-ion batteries, because of their high energy density and relatively low environmental pollution, are widely used in electronic devices, power systems, and electric vehicles [3]. An effective battery management system (BMS) is vital for ensuring the reliable operation of electric vehicles [4]. State of charge (SOC) is defined as the ratio of the remaining capacity of a battery to its fully charged capacity after a period of use or prolonged storage [5]. Accurate SOC estimation is the basis for enabling other BMS functions. State of health (SOH) represents the health status of a battery and reflects changes in its internal resistance and capacity, providing an indicator of battery aging [6]. Accurate SOC and SOH estimation are both critical for ensuring the safe operation of electric vehicles and extending their service life [7]. Currently, many SOC and SOH estimation methods focus on individual cells, however, EV batteries consist of numerous cells connected in various series and parallel configurations [8]. This inevitably influences SOC and SOH estimation accuracy. Therefore, accurate estimation of SOC and SOH in battery packs remains a relatively new and important research area [9].

There are currently three commonly used SOC estimation methods for battery packs. The first method focuses on the changes and inconsistencies between battery cells and estimates the battery pack SOC by averaging the SOC values of individual cells [10, 11]. However, this approach typically involves extensive computation, which

limits its practicality for real-time applications [8]. The second method adopts a data-driven approach, in which SOC is estimated from operating data through trained models [3]. Although effective, this method usually requires large datasets for training and validation, which can be resource-intensive [12, 13]. The third method treats the module as a single large-capacity battery [4, 14], which reduces computational demand and simplifies model construction.

In general, battery models can be categorized as electrochemical models (EMs), neural network models and equivalent circuit models (ECMs). EMs offer high accuracy but demand considerable computational resources [15]. Neural network models are data-driven approaches that rely on extensive experimental testing to collect large battery datasets for training [16]. ECMs, by contrast, are widely used in electric vehicles due to their simple structure and low computational requirements [4, 17]. Typically, an ECM consists of interconnected resistive and capacitive elements, with common equivalent circuit models including the Rint model [18], the Thevenin model [19], and the DP model [20]. As the RC network increases, the accuracy of the model improves, but the model complexity also increases, making it difficult to apply in actual vehicle conditions. [21]. Therefore, it is necessary to reach an appropriate balance between model accuracy and complexity.

The capacity testing method is a commonly used approach for SOH estimation [22], as it directly evaluates the SOH of the battery pack by measuring its capacity. However, this method requires a long testing period and is often measured in the laboratory. Data-driven method is another widely applied approach [23, 24]. Although it can achieve high estimation accuracy, it does not explicitly account for battery's underlying physical or chemical mechanisms, making it difficult to reveal how external factors influence aging behavior [7]. Another typical SOH estimation method is joint estimation. Since SOC and SOH are strongly interdependent, the estimation results of SOC will also affect the estimation results of SOH. Thus, joint estimation of SOC and SOH is crucial for improving overall accuracy [25-27]. To achieve this, Hu et al. proposed an NSSR-LSTM neural network to perform the joint estimation of SOC and SOH [28]. Tang et al. adopted a "leader-follower" strategy to jointly estimate the SOC

and SOH of the battery pack [25]. Yu et al. applied the DEKF algorithm for SOC estimation in series-parallel battery packs [29]. Park et al. used combined adaptive extended Kalman filtering (AEKF) combined with single forgetting factor ratio partial capacity recursive least squares (SPCSFFRLS) to estimate both SOC and SOH, achieving significantly higher accuracy than the AEKF method [30]. Xu et al. proposed a double-fuzzy adaptive extended Kalman filter for joint SOC-SOH estimation [31]. However, these methods still suffer from truncation errors, which reduce estimation accuracy. The particle filter (PF) algorithm, by contrast, relies on the Monte Carlo algorithm, where the weight of each particle represents the probability density function [32]. ts main advantages include ease of implementation, the absence of truncation errors, and improved estimation accuracy. Zhong et al. applied the PF algorithm to estimate the SOC of battery packs with series and parallel configurations, achieving highly accurate results [33]. Chen et al. estimated the SOC of the battery pack through PF algorithm [34]. Hao et al. used unscented particle filtering (UPF) to estimate the SOC of the battery [35]. Zhang et al. used a PF algorithm to estimate the SOH of the battery pack, and verified the effectiveness of this method through the new European driving condition curve and dynamic test curve [36]. Shi et al. used an improved UPF to estimate battery pack SOH [37]. Dong et al. modeled battery SOH decay as Brownian particle motion and applied a PF-based framework to evaluate battery health [38]. Xu et al. proposed a dual-particle filter joint estimation algorithm for SOC and SOH of a single battery, achieving high accuracy [39]. Since the accuracy of the particle filter algorithm is highly sensitive to initial values, accurate initialization becomes particularly important. The particle swarm optimization (PSO) algorithm, noted for its robustness and global search ability, provides an effective solution [40]. The PSO algorithm has been widely employed to optimize the initial parameters of the model [41]. Zheng et al. employed PSO algorithm to identify parameters and subsequently estimated the SOC of the battery pack using the extended Kalman filter (EKF) [42]. Zhang et al. applied the PSO algorithm to improve the radial basis function neural network estimation model, thereby improving estimation accuracy [8].

Based on the review, this study develops four battery packs with different

connection configurations, jointly estimates their SOC and SOH, and analyzes performance differences among them. Considering that the dual particle filter algorithm is sensitive to initial value, the particle swarm optimization algorithm is implemented to optimize the initial parameters for the PF algorithm, thereby enabling more accurate joint SOC-SOH estimation.

The remaining content of this article is organized as follows. Section 2 describes the experimental platform for battery pack testing and presents the construction of equivalent circuit models derived from single-cell models. Section 3 analyzes the performance differences in capacity and open circuit voltage across four battery-pack connection configurations, optimizes their initial parameters using PSO algorithm, and provides validation. Section 4 applies the dual particle filter algorithm for joint SOC-SOH estimation of four different battery packs, compares the results with those of the DEKF algorithm and the EKF algorithm, and verifies SOC estimation accuracy under Dynamic Stress Test (DST) conditions.

2. Experiment

An experimental platform was established to evaluate battery pack performance under controlled conditions. The setup comprises a temperature chamber maintained at a constant 25°C to ensure consistent room-temperature comparisons across different packs. Charge–discharge cycling was conducted using a LAND CT6001BM battery test system, which provides a maximum output of 60 V and 50 A, thereby satisfying the discharge requirements of all tested modules. The Samsung INR18650-35E cell was selected as the subject of this study, with its key performance parameters detailed in Table 1."

Table 1 Performance parameters of the single cell

parameter name	value	unit
Nominal capacity	3400	mAh
Nominal voltage	3.60	V
Upper cut-off voltage / lower cut-off voltage	2.65~4.2	V
Charging current	1700	mAh
Maximum charge current	2000	mAh

Maximum discharge current (continuous discharge)	8000	mAh
Maximum discharge current (non-continuous discharge)	13000	mAh

To systematically investigate the performance disparities arising from various topological arrangements, this study constructed four distinct battery pack configurations utilizing a total of 32 individual cells, as schematically illustrated in Fig. 1. Specifically, Fig. 1(a) depicts the 4S2P architecture, wherein the assembly is formed by connecting two modules in parallel, with each module comprising four cells linked in series. Conversely, Fig. 1(b) presents the 2P4S configuration, characterized by four parallel pairs connected in series; in this arrangement, cells are initially grouped into parallel duals before being integrated into a series string. Furthermore, to examine the extremes of connectivity, Fig. 1(c) illustrates an 8S1P setup where all eight constituent cells within the module are arranged exclusively in series. Finally, Fig. 1(d) demonstrates the 8P1S topology, in which the eight cells are connected entirely in parallel. These diverse configurations enable a comprehensive comparative analysis of how series and parallel interconnections influence the overall electrochemical behavior and consistency of the battery packs.

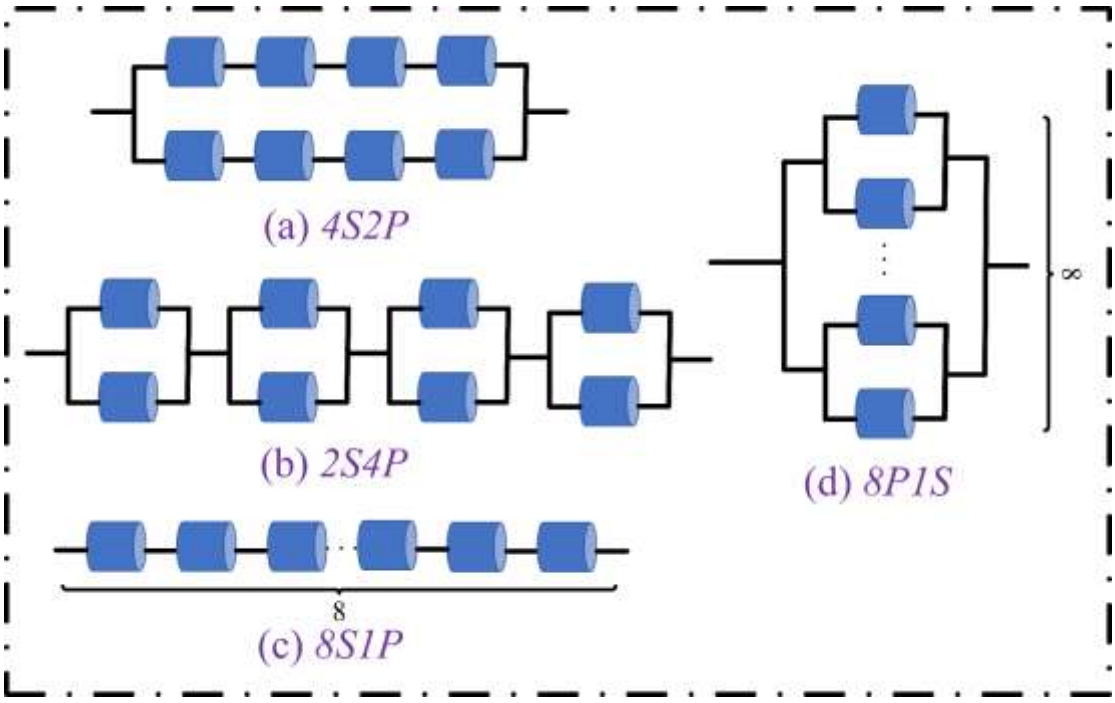


Fig. 1. Schematic diagrams illustrating the four distinct topological configurations of

the battery pack interconnections

As battery packs undergo prolonged cycling and aging, inevitable heterogeneity emerges in critical performance metrics, specifically regarding cell capacity and internal resistance [43, 44]. These discrepancies are not static; rather, they tend to exacerbate progressively over the operational lifespan of the system. To rigorously investigate the performance divergence among various battery modules, it is imperative to establish precise definitions for key state indicators, namely the State of Charge (SOC), State of Health (SOH), and total capacity of the pack. Consequently, the foundational step involves quantifying the SOC and SOH for each individual cell within the assembly, the mathematical formulations for which are explicitly delineated in Equation 1 and Equation 2, respectively.

$$SOC = \frac{C_r}{C_l} \times 100\% \quad (1)$$

$$SOH = \frac{C_c}{C_f} \quad (2)$$

where C_r represents the current remaining capacity, C_l represents the maximum available capacity, C_c represents the current rated capacity and C_f represents the nominal capacity of the new battery.

2.1 Series battery pack

In a series-connected battery pack comprising n individual cells, let the SOC of the i-th cell be denoted as SOC_i, respectively. Due to the inherent "barrel effect" governing series configurations, the overall usable capacity of the pack is fundamentally constrained by the cell possessing the minimum available remaining capacity. This limitation is critical for operational safety, as it prevents the system from subjecting specific cells to detrimental over-discharge or overcharge conditions [8, 45]. Consequently, the effective capacity of the series battery pack is mathematically defined by Equation 3. In alignment with established literature, the SOH is characterized according to the formulation presented in Equation 4 [29], while the specific calculation methodology for SOH adopted in this study is explicitly detailed in Equation 5 [33].

$$C_p = \min_{1\le i\le n}(C_i \times SOC_i) + \min_{1\le j\le n}(C_j \times (1 - SOC_j)) \quad (3)$$

$$SOC_P = \frac{\min_{1\le i\le n}(C_i \times SOC_i)}{\min_{1\le i\le n}(C_i \times SOC_i) + \min_{1\le j\le n}(C_j \times (1 - SOC_j))} \quad (4)$$

$$SOH_p = \frac{C_p}{C_f} = \frac{\min_{1\le i\le n} C_i}{C_f} \quad (5)$$

where C_p represents the nominal capacity of the battery pack.

2.2 Parallel battery pack

In contrast to series configurations, a parallel battery pack consisting of n individual cells allows for the complete utilization of each cell's energy storage potential, as the parallel topology mitigates the risk of premature cutoff due to single-cell voltage limits. Consequently, the discharge rated capacity and SOC for each constituent cell are denoted as C_i and SOC_i, respectively. Under these conditions, the total available capacity of the parallel assembly is defined as the summation of the individual cell capacities, as mathematically expressed in Equation 6. Furthermore, the aggregate SOC of the parallel battery pack is calculated based on the ratio of total remaining charge to total rated capacity, as illustrated in Equation 7. Finally, the SOH for the parallel configuration is formulated according to Equation 8, reflecting the cumulative health status of the parallelized modules.

$$C_p = \sum_{i=1}^{n} C_i \quad (6)$$

$$SOC_p = \frac{\sum_{i=1}^{n} C_i \times SOC_i}{\sum_{i=1}^{n} C_i} \quad (7)$$

$$SOH_P = \frac{\sum_{i=1}^{n} C_i}{C_f} \quad (8)$$

2.3 Hybrid battery pack

In practical electric vehicle deployments, battery packs are predominantly configured using hybrid topologies that strategically combine series and parallel connections to simultaneously elevate system voltage and augment total energy

capacity. Generally, two distinct architectural strategies are employed: the series-parallel configuration (cells connected in series first, then paralleled) and the parallel-series configuration (cells connected in parallel first, then serialized). This study specifically focuses on the parallel-series arrangement, wherein mm individual cells are initially aggregated into parallel modules, followed by the series connection of nn such modules to form the complete pack. Let the nominal capacity and SOC of each constituent cell be denoted as C_{ij} and SOC_{ij}, respectively. Based on this topology, the aggregate capacity, overall, SOC, and SOH of the hybrid battery pack are rigorously formulated and presented in Equation 9, Equation 10, and Equation 11, respectively.

$$C_i = \sum_{j=1}^{m} C_{ij} \quad (9)$$

$$SOC_i = \frac{\sum_{j=1}^{m} C_{ij} \times SOC_{ij}}{\sum_{j=1}^{m} C_{ij}} \quad (10)$$

$$SOH_i = \frac{\sum_{j=1}^{m} C_{ij}}{C_f} \quad (11)$$

Subsequently, n of these parallelized modules are interconnected in series to constitute the final battery pack architecture. In this parallel-then-series configuration, the resultant system-level metrics—specifically the total pack capacity, the aggregate SOC, and the overall SOH—are derived by synthesizing the characteristics of the individual parallel groups. These critical performance parameters are denoted as Cps, SOC_{ps}, and SOH_{ps}, respectively. The mathematical formulations governing the calculation of these composite values are explicitly detailed in Equation 12, Equation 13, and Equation 14, which account for the cumulative effects of both the parallel aggregation and the subsequent series integration.

$$C_{ps} = \min_{1 \le i \le n}(C_i \times SOC_i) + \min_{1 \le k \le n}(C_k \times (1 - SOC_k)) \quad (12)$$

$$SOC_{ps} = \frac{\min_{1 \le i \le n}(C_i \times SOC_i)}{\min_{1 \le i \le n}(C_i \times SOC_i) + \min_{1 \le k \le n}(C_k \times (1 - SOC_k))} \quad (13)$$

$$SOH_{ps} = \frac{C_p}{C_f} = \frac{\min_{1 \le i \le n} C_i}{C_f} \quad (14)$$

where C_k indicates the maximum usable capacity for charging, and C_f indicates the rated capacity of the new battery pack.

Similarly, for mSnP battery pack that are first connected in series and then n in parallel, the capacity, SOC, and SOH are represented by Eq. 15, Eq. 16, and Eq. 17.

$$C_{sp} = \sum_{i=1}^{n} \left\{ \min_{1 \le j \le m} (C_{ij} \times SOC_{ij}) + \min_{1 \le k \le m} (C_{ik} \times (1 - SOC_{ik})) \right\} \quad (15)$$

$$SOC_{sp} = \frac{\sum_{i=1}^{n} \left\{ \min_{1 \le j \le m} (C_{ij} \times SOC_{ij}) + \min_{1 \le k \le m} (C_{ik} \times (1 - SOC_{ik})) \right\} \times SOC_i}{\sum_{i=1}^{n} \left\{ \min_{1 \le j \le m} (C_{ij} \times SOC_{ij}) + \min_{1 \le k \le m} (C_{ik} \times (1 - SOC_{ik})) \right\}} \quad (16)$$

$$SOH_{sp} = \frac{\sum_{i=1}^{n} \left\{ \min_{1 \le j \le m} (C_{ij} \times SOC_{ij}) + \min_{1 \le k \le m} (C_{ik} \times (1 - SOC_{ik})) \right\}}{C_f} \quad (17)$$

where C_f represents the nominal capacity of the new battery pack and SOC_{i} represents the SOC of a series module.

3. Battery pack performance analysis

To systematically investigate the discrepancies in energy storage capabilities arising from different topological configurations, comprehensive capacity characterization tests were conducted on the fabricated battery packs. The empirical results of these experiments are graphically summarized in Fig. 2. Quantitative analysis reveals distinct variations in the measured capacities across the four configurations: the purely parallel assembly exhibited the highest capacity at 26.32 Ah, whereas the series-only configuration yielded the lowest value of 3.299 Ah. Furthermore, the hybrid architectures demonstrated intermediate performance levels, with the parallel-series and series-parallel arrangements registering measured capacities of 6.549 Ah and 6.577 Ah, respectively. These findings underscore the significant impact of connection topology on the overall usable capacity of the battery system.

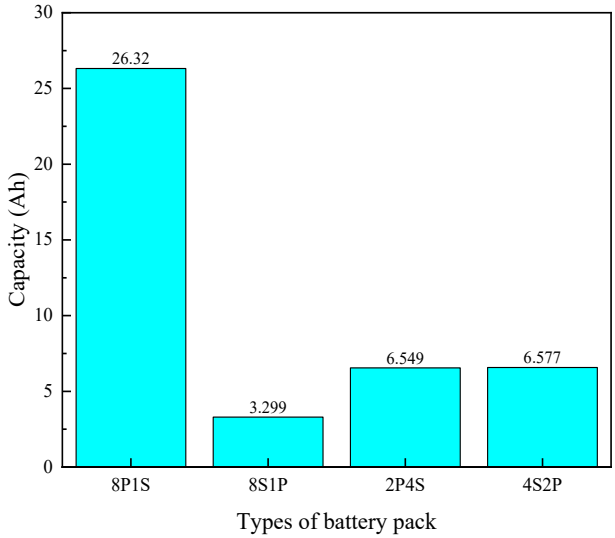
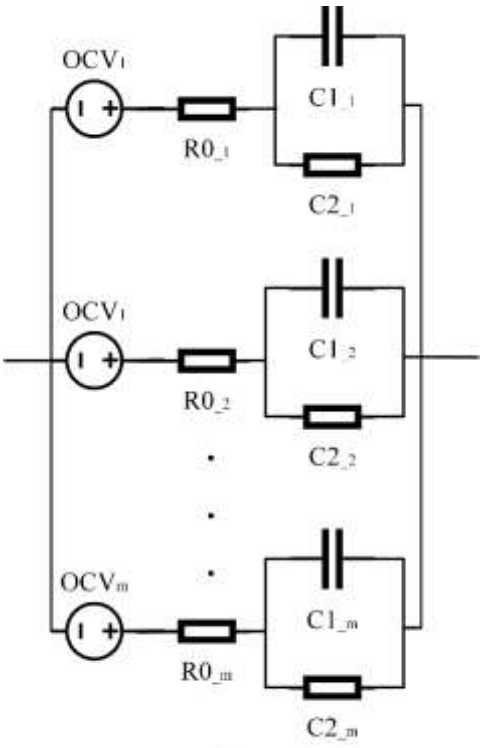
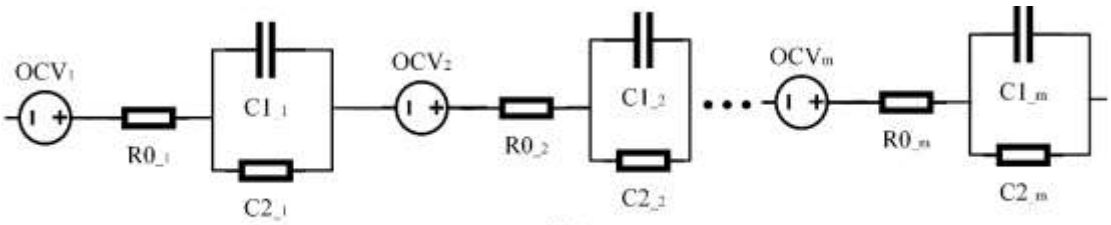


Fig. 2 Comparative Analysis of Capacity Characteristics Across Diverse Battery Pack Topologies

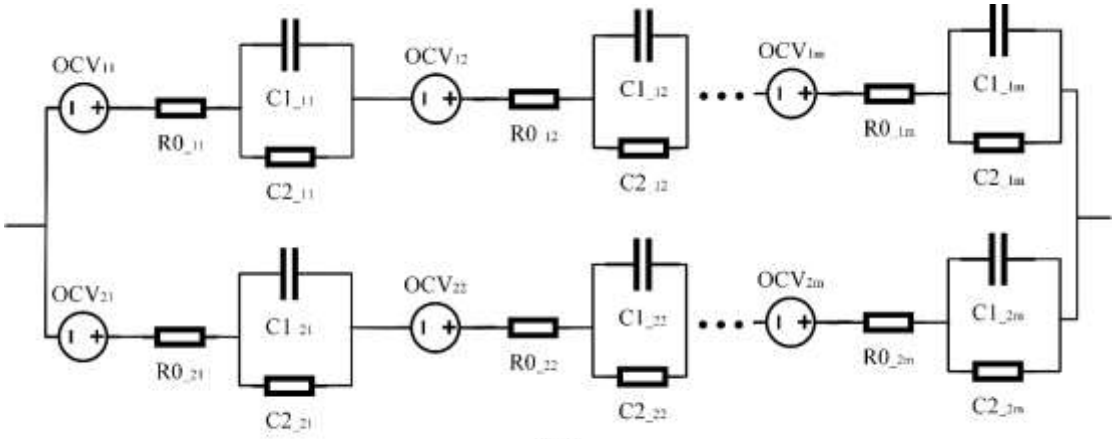
The Equivalent Circuit Model (ECM) represents a widely adopted electrical abstraction that utilizes fundamental circuit elements—specifically resistors, inductors, and capacitors—to emulate the complex dynamic behavior and transient responses of lithium-ion batteries [19, 21]. Structurally, a typical ECM comprises an ohmic internal resistance connected in series with one or more parallel resistor-capacitor (RC) networks, which account for polarization effects [20]. In this study, a strategic trade-off was made between model fidelity and computational complexity; consequently, a first-order RC network configuration was selected for implementation. This specific architecture, known as the Thevenin model, consists of a single ohmic resistor in series with one RC parallel branch. Leveraging the Thevenin equivalent parameters identified for individual cells, comprehensive models for various battery pack configurations were subsequently constructed. The schematic representation of the employed Thevenin model is illustrated in Fig. 3.


OCV1
R0_1
C1_1
C2_1
OCV1
R0_2
C1_2
C2_2
OCVm
R0_m
C1_m
C2_m

(a)


OCV1
R0_1
C1_1
C2_1
OCV2
R0_2
C1_2
C2_2
OCVm
R0_m
C1_m
C2_m

(b)


OCV11
R0_11
C1_11
C2_11
OCV12
R0_12
C1_12
C2_12
OCV1m
R0_1m
C1_1m
C2_1m
OCV21
R0_21
C1_21
C2_21
OCV22
R0_22
C1_22
C2_22
OCV2m
R0_2m
C1_2m
C2_2m

(c)

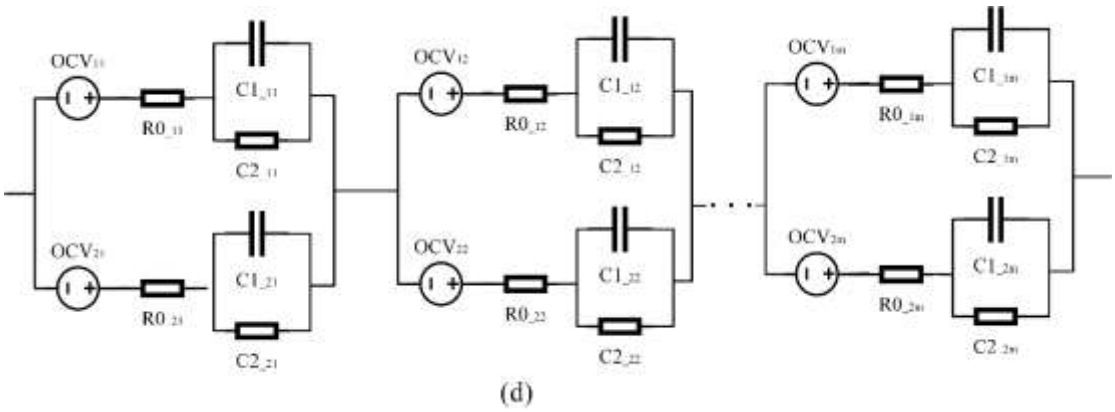


Fig. 3 Schematic representations of the equivalent circuit models for diverse battery pack topologies: (a) parallel configuration; (b) series configuration; (c) series-parallel arrangement; (d) parallel-series architecture

The mathematical formulations governing the aggregate open-circuit voltage (OCV), equivalent internal resistance, and equivalent capacitance for battery packs configured in series are explicitly defined by Equation 18. Conversely, the corresponding expressions used to derive these equivalent parameters for parallel-connected battery pack architectures are presented in Equation 19 [4]. These equations provide the theoretical foundation for scaling single-cell model parameters to multi-cell pack configurations based on their specific topological arrangements.

$$\begin{cases} \mathrm{OCV}_{(se)} = \sum_{i}^{m} \mathrm{OCV}_i \\ R_{0(se)} = \sum_{i}^{m} R_{0_i} \\ R_{1(se)} = \sum_{i}^{m} R_{1_i} \\ C_{1(se)} = C_{1_1} = C_{1_2} = \cdots = C_{1_m} \end{cases} \tag{18}$$

$$\begin{cases} \mathrm{OCV}_{(pa)} = \mathrm{OCV}_1 = \mathrm{OCV}_2 = \cdots = \mathrm{OCV}_m \\ R_{0(pa)} = \dfrac{1}{\sum_{i}^{m} 1/R_{0_i}} \\ R_{1(pa)} = \dfrac{1}{\sum_{i}^{m} 1/R_{1_i}} \\ C_{1(pa)} = \sum_{i}^{m} C_{1_i} \end{cases} \tag{19}$$

where OCV_i , R_{0_i}, R_{1_i} and C_{1_i} $(i \in 1,2\ldots\ \mathrm{m})$. represent the open circuit voltage,

ohmic internal resistance, polarization internal resistance and polarization capacitance of the single cell in the battery pack, respectively.

In an analogous manner, for battery packs configured in a series-parallel topology, the equivalent parameters—specifically the open-circuit voltage, internal resistance, and capacitance—are first determined for the individual series strings. Subsequently, each completed series string is abstracted as a single equivalent cell, allowing the overall pack characteristics to be derived by applying the standard parallel connection formulations. Conversely, for packs arranged in a parallel-series configuration, the calculation procedure is inverted: the equivalent parameters are initially computed for the parallel groups. These parallel clusters are then treated as unified equivalent cells, upon which the series connection equations are applied to ascertain the final aggregate properties of the entire battery pack.

In this study, the Particle Swarm Optimization (PSO) algorithm is employed to perform precise parameter identification for the battery pack models. Distinguished by its inherent capabilities for self-organization, evolutionary adaptation, and robust global search efficiency, PSO has proven highly effective in solving complex optimization problems [41]. The algorithm conceptually mimics the stochastic foraging behavior of bird flocks, wherein each particle (representing a potential solution) iteratively updates its velocity and position within the search space based on both its own historical best experience and the global best found by the swarm. This dynamic adjustment process continues until convergence criteria are satisfied, utilizing a predefined fitness function to evaluate and determine the attainment of the optimal solution [40, 46]. The mathematical formulation governing the velocity and position updates of the particles is explicitly defined in Equation 20.

$$f = \sqrt{\sum_{i=1}^{N} \left| Y(i) - y(i) \right|} \quad (20)$$

where: $Y(i)$ Represents the optimized output value, $y(i)$ Represents the actual measured value of the data.

The identification results are shown in Table. 2. As the number of series connections increases, the equivalent resistance of the battery pack will also increase.

As the number of parallel connections increases, the equivalent capacitance also increases and so does the value of the open circuit voltage, as shown in Fig. 4. Among them, the open circuit voltages of 2P4S and 4S2P are basically the same.

Table. 2 Identification results of different battery packs

	R_0 (Ω)	R_1 (Ω)	C_1 (F)
8P1S	0.0064	0.0051	10177
8S1P	0.2500	0.2907	1048.5
2P4S	0.0650	0.0810	3997.9
4S2P	0.0789	0.0810	4053.5

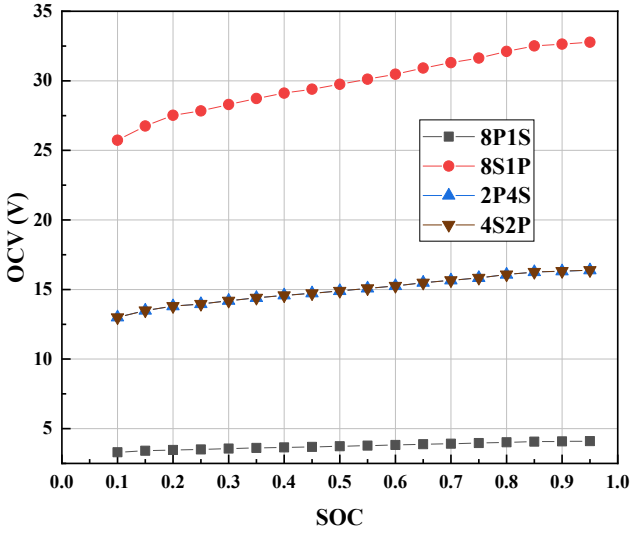


Fig. 4 Open circuit voltage of different battery packs

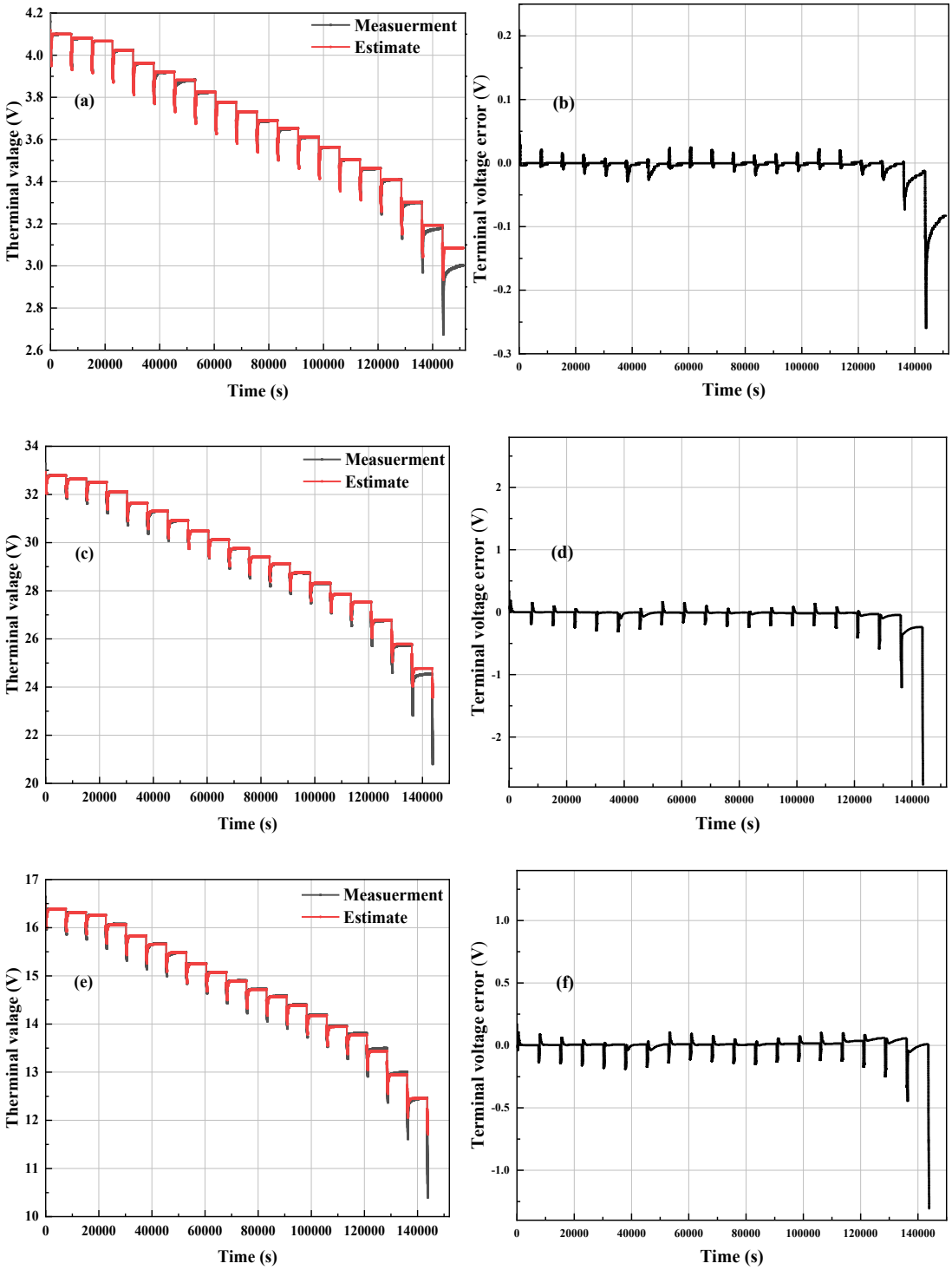
The terminal voltage error is shown in Table. 3 and the terminal voltage is used to verify the accuracy of the model, as shown in Fig. 5.

Table. 3 Terminal voltage error of different battery packs

	8P1S	8S1P	2P4S	4S2P
RMSE (V)	0.02507	0.0867	0.0405	0.0482
MAE (V)	0.0089	0.0356	0.0230	0.0169

As depicted in Fig. 5 and presented in Table 3, a notable trend emerges: with the augmentation in the quantity of batteries connected in series, there is a concurrent rise in the terminal voltage error. Concurrently, the duration required to attain the cut-off voltage diminishes. This phenomenon can be attributed to the cumulative error that arises when multiple batteries are linked in series. Consequently, when interconnecting individual cells in series, it is imperative to carefully deliberate on an appropriate

number of series connections. While series connection offers the advantage of elevating the overall voltage, it simultaneously leads to a reduction in the discharge time.



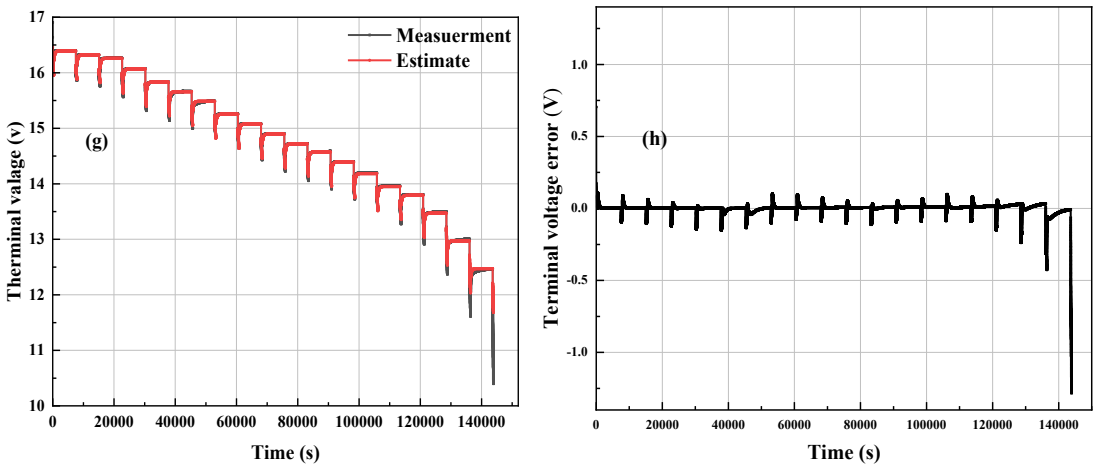


Fig. 5 Terminal voltage and error of battery packs with different connection methods. (a) and (b) Parallel connection, (c) and (d) Series connection, (e) and (f) parallel-series connection, (g) and (h) series-parallel connection

3.1 Joint estimation of SOC and SOH

The particle filter technique implements recursive Bayesian filtering by leveraging non-parametric Monte Carlo simulation approaches [47]. It is suitable for any nonlinear system that can be characterized using a state space model. When compared to Gaussian models, particle filters exhibit broader applicability and superior modeling capabilities. The fundamental concept involves employing a set of dispersed random sampling points to approximate the posterior probability density function of the system state. Subsequently, the sample mean is utilized as a substitute for integral computation [35]. Through this method, the minimum variance estimate of the final state can be achieved. The DPF algorithm extends this methodology to facilitate the joint estimation of the SOC and SOH. Specifically, it generates one set of particles for SOC estimation and another set for SOH estimation [31]. The procedural steps of the DPF algorithm are outlined in Table 4.

Table. 4 The procedure of DPF algorithm

1 Particle initialization: randomly generate two groups of particles $\{x_0^i\}_1^N$, $\{\theta_0^j\}_1^N$. At this time, the weight of each particle is 1/N. are used to estimate SOC and SOH respectively.
2 Importance sampling: based on parameters of the equivalent circuit model $\hat{\theta}_k = [R_0 \quad C]$ and equation of state x_k , the observation value y_k at time k is obtained and then Reassign weights

to the particle set $\{x_k^i\}_1^N$ and normalize it.

$$\omega_k^i = \omega_{k-1}^i \frac{p(y_k^i \mid x_k^i) p(x_k^t \mid x_{k-1}^i)}{q(x_k^i \mid x_{k-1}^i, y_{1:k})}$$

$$\omega_k^j = \omega_{k-1}^j \frac{p(y_k^j \mid x_k^j) p(x_k^t \mid x_{k-1}^j)}{q(x_k^j \mid x_{k-1}^j, y_{1:k})}$$

$$\omega_k^i = \frac{\omega_k^i}{\sum_{i=1}^N \omega_k^i}$$

$$\omega_k^j = \frac{\omega_k^j}{\sum_{i=1}^N \omega_k^j}$$

3 Resampling: Compare the effective particle number with the preset threshold. If the effective particle number is less than the set threshold, resampling is performed. The effective particle number calculation is expressed by the formula.

$$\hat{N}_{eff}^i = 1 \Big/ \sum_{i=1}^N (\omega_k^i)^2$$

$$\hat{N}_{eff}^j = 1 \Big/ \sum_{j=1}^N (\omega_k^j)^2$$

From the weights obtained in the second step, remove particles with smaller weights and copy particles with larger weights to obtain a new particle set. The weights of all particles are 1/N. Let $k = k + 1$ and go back to the second step.

4 Output results: If the set threshold conditions are met, the results will be output.

$$SOC_k = \sum_{i=1}^N \omega_k^i x_k^i$$

$$SOH_k = \sum_{j=1}^N \omega_k^j \theta_k^j$$

The parameters that have been determined through the PSO algorithm are employed as the initial parameter values for the DPF algorithm. A flowchart depicting the operational sequence of the combined PSO-DPF algorithm is presented in Fig. 6.

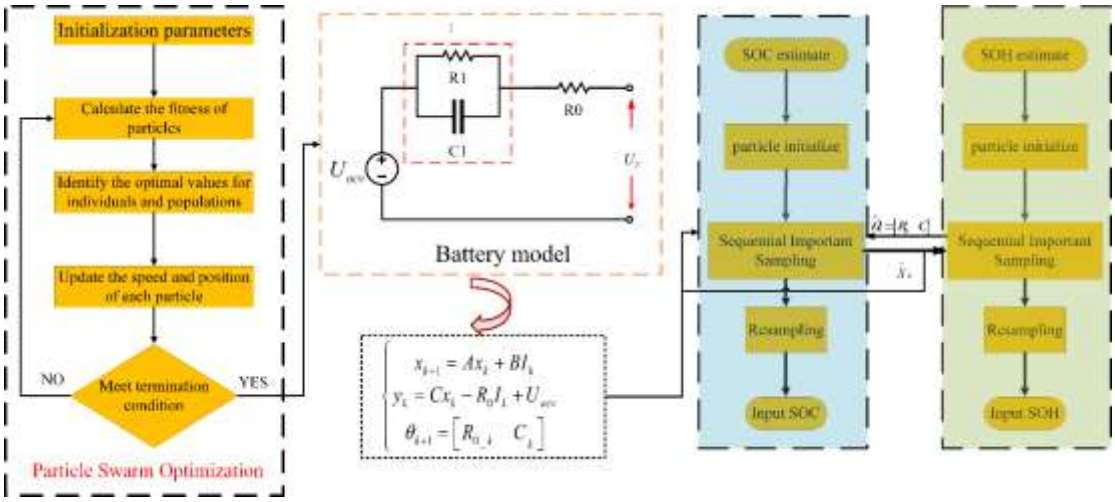
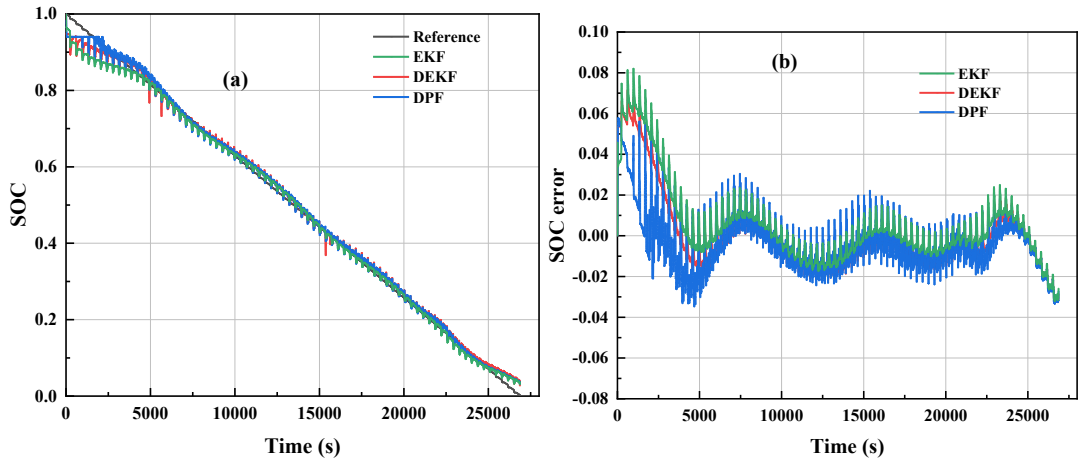


Fig. 6 The flowchart of PSO-DPF algorithm

The verification process was conducted under DST operating conditions, as illustrated in Fig. 7. The results demonstrate that, for battery packs configured with four distinct connection methods, the RMSE and MAE values associated with the DPF algorithm were consistently lower than those obtained using the DEKF algorithm, which itself outperformed the standard EKF algorithm. Consequently, the DPF algorithm achieved the highest level of estimation accuracy among the three methods evaluated. Furthermore, the error observed in the series circuit configuration was the highest, primarily attributable to the accumulation of errors over time. In contrast, the error associated with the battery pack connected in a parallel-series arrangement was found to be lower than that of the battery pack connected in a series-parallel configuration. Therefore, when designing the connection of battery packs, opting for a parallel-series connection is recommended to achieve better performance.



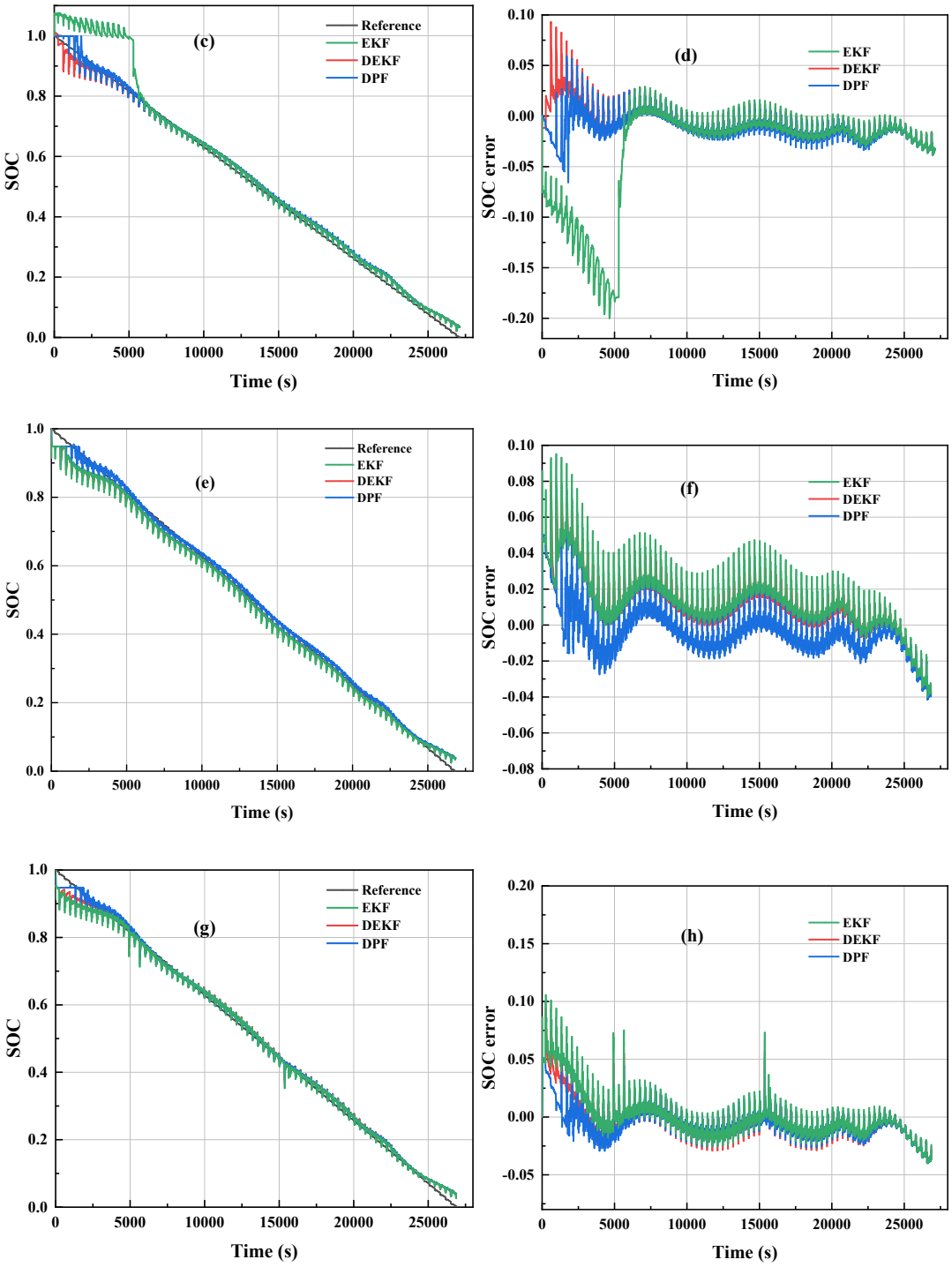


Fig. 7 SOC estimation results and errors of different battery packs. (a) and (b) Parallel connection, (c) and (d) Series connection, (e) and (f) parallel-series connection, (g) and (h) series-parallel connection

Table. 5 SOC estimation errors of different battery packs

	8P1S			8S1P			2P4S			4S2P		
	EKF	DEKF	DPF	EKF	DEKF	DPF	EKF	DEKF	DPF	EKF	DEKF	DPF
RMSE	0.0207	0.0190	0.0149	0.0367	0.0181	0.0175	0.0237	0.0204	0.0144	0.0208	0.0180	0.0147

MAE	0.0131	0.0130	0.0114	0.0364	0.0152	0.0150	0.0182	0.0150	0.0109	0.0144	0.0136	0.0118

The temporal evolution of the SOH is depicted in Fig. 8. DST operating conditions, the SOH of four distinct battery module configurations—parallel connection, series connection, parallel-series connection, and series-parallel connection—experienced declines of 0.21%, 0.58%, 0.40%, and 0.48%, respectively. These findings suggest that the series configuration demonstrates the most rapid degradation in SOH when subjected to the same operating conditions. Moreover, the rate of SOH attenuation for the battery pack connected in a parallel-series arrangement was found to be lower compared to that of the battery pack connected in a series-parallel configuration, highlighting the relative advantage of the former in terms of preserving battery health over time.

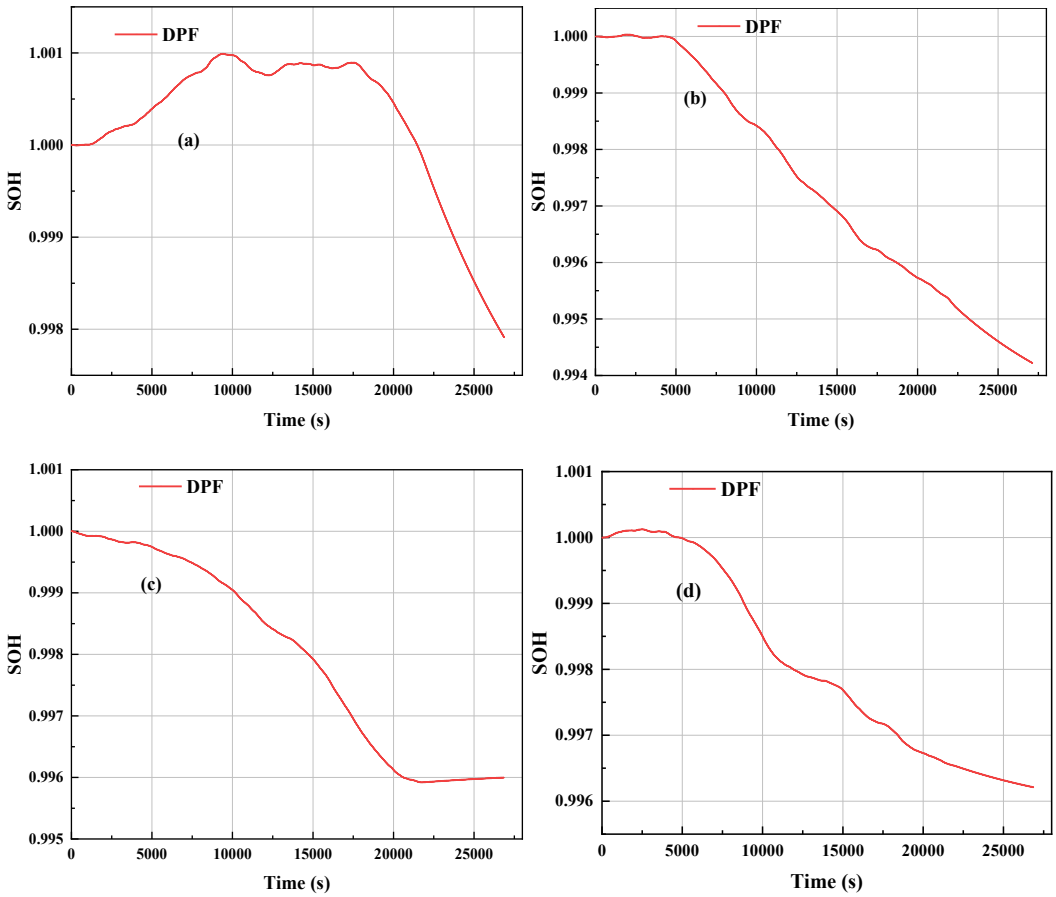


Fig. 8 SOH estimation results of different battery packs. (a) Parallel connection, (b) Series connection, (c) parallel-series connection, (d) series-parallel connection

4. Conclusion

This study develops equivalent circuit models for battery packs configured in four distinct topologies to evaluate their performance disparities. A DPF framework is subsequently implemented for the joint estimation of SOC and SOH. Furthermore, the PSO algorithm is employed to optimize the model's initial parameters, which are then integrated into the DPF procedure. The primary conclusions of this work are summarized as follows:

(1) The PSO algorithm was employed to optimize the initial parameters for the four battery pack configurations, with validation performed against terminal voltage measurements. The results indicate a positive correlation between the number of series-connected cells and model error; however, the MAE for all configurations remained below 10 mV. These findings demonstrate that the PSO algorithm achieves high estimation accuracy, establishing a robust foundation for subsequent SOC and SOH estimation.

(2) Comparative analysis revealed that the series-connected pack exhibited the highest estimation error, whereas the parallel–series configuration demonstrated superior accuracy compared to the series–parallel arrangement. Notably, both the RMSE and MAE for SOC remained below 2% across all tests. These findings underscore the high accuracy and robustness of the DPF algorithm, offering valuable insights for future research on lithium-ion battery packs.

(3) The DPF algorithm was employed to estimate the SOH of four distinct battery modules under DST conditions. The results indicate a positive correlation between the number of series-connected cells and the rate of SOH attenuation. Specifically, the pack comprising eight series-connected cells exhibited an SOH decline of 0.53%. Furthermore, the parallel–series configuration demonstrated a lower degradation rate compared to the series–parallel arrangement. These findings suggest that prioritizing parallel connections prior to series grouping during battery pack design can effectively mitigate degradation and extend the service life of electric vehicles.

Declaration of interest statement

The authors declare that they have no known competing financial interests or

personal relationships that could have appeared to influence the work reported in this paper.

Credit author statement

Nana Zhou: Conceptualization, Experiment, Validation, Writing - Original Draft. Lianfeng Lai: Resources, Methodology, Writing - Review & Editing; Zhihui Deng: Methodology, Validation, Supervision. Fengjun Zhou: Conceptualization, Experiment. Bing Lu: Writing - Review & Editing, Resources. Weiwei Huo: Supervision, Validation, Supervision; Yonghong Xu: Experiment, Software, Writing - Review & Editing.

Funding

This work was sponsored by the High Level Talent Start up fund of Shandong XieHe University (SDXHQD2025089), the Open Fund Project of Vehicle Measurement, Control and Safety Key Laboratory of Sichuan Province (QCCK2025-0012) and National Natural Science Foundation of China (Grant No. 52402464).

Data Availability

The data that support the findings of this study are available from the corresponding author upon reasonable request.

Reference

[1] Goodenough JB, Park K-S. The Li-Ion Rechargeable Battery: A Perspective. Journal of The American Chemical Society. 2013; 135:1167-11176.
[2] Wu FX, Maier J, Yu Y. Guidelines and trends for next-generation rechargeable lithium and lithium-ion batteries. Croyal Society of Chemistry. 2020; 49: 1569-1614.
[3] Ragone M, Yurkiv Y, Ramasubramanian A, Kashir B. Data driven estimation of electric vehicle battery state-of-charge informed by automotive simulations and multi-physics modeling. Journal of Power Sources. 2021; 483: 229108.
[4] Kim J, Cho BH. Screening process-based modeling of the multi-cell battery string in series and parallel connections for high accuracy state-of-charge estimation. Energy. 2013; 57: 581-599.
[5] Yang CF, Wang XY, Fang QH, Dai HF, Cao YQ, Wei XZ. An online SOC and capacity estimation method for aged lithium-ion battery pack considering cell inconsistency. Journal of Energy Storage. 2020; 29: 101250.

[6] Han XB, Lu LG, Zheng YJ, Feng XN, Li Z, Li JQ, Ouyang MG. A review on the key issues of the lithium-ion battery degradation among the whole life cycle. eTransportation. 2019; 1:100005.
[7] Tian JQ, Liu XH, Li SQ, Wei ZB, Zhang X, Xiao GX, Wang P. Lithium-ion battery health estimation with real-world data for electric vehicles. Energy. 2023; 270: 126855.
[8] Zhang GY, Xia BZ, Wang JM, Ye B, Chen YC, Yu ZJ, Li YH. Intelligent state of charge estimation of battery pack based on particle swarm optimization algorithm improved radical basis function neural network. Journal of Energy Storage.2022; 50: 104211.
[9] Wang Z, Gladwin DT, Smith MJ, Haass S. Practical state estimation using Kalman filter methods for large-scale battery systems. Applied Energy. 2021; 294: 117022.
[10] Zheng YJ, Gao WK, Ouyang MG, Lu LG, Zhou L, Han XB. State-of-charge inconsistency estimation of lithium-ion battery pack using mean-difference model and extended Kalman filter. Journal of Power Sources. 2018; 383: 50-80.
[11] Dong HN, Huang W, Zhao LX. Low complexity state-of-charge estimation for lithium-ion battery pack considering cell inconsistency. Journal of Power Sources. 2021; 515: 230599.
[12] Finegan DP, Zhu J, Feng XN, Keyser M, Ulmefors M, Li W, Bazant MZ, Cooper SJ. The Application of Data-Driven Methods and Physics-Based Learning for Improving Battery Safety. Joule.2021; 5: 316-329.
[13] Manoharan A, Sooriamoorthy D, Begam KM, Aparow VR. Electric vehicle battery pack state of charge estimation using parallel artificial neural networks. Journal of Energy Storage. 2023; 72: 108333.
[14] Zhou SY, Chen ZQ, Huang DY, Lin TT. A Fault-Tolerant SoC Estimation Method for Series–Parallel Connected Li-Ion Battery Pack. IEEE TRANSACTIONS ON POWER ELECTRONICS. 36(12): 13434-13448.
[15] Tran M-K, Mathew M, Janhunen S, Panchal S. A comprehensive equivalent circuit model for lithium-ion batteries, incorporating the effects of state of health, state of charge, and temperature on model parameters. Journal of Energy Storage.2021; 43:103252.
[16] Naseri F, Schaltz E, Stroe D-L, Gismero A, Farjah E. An Enhanced Equivalent Circuit Model With Real-Time Parameter Identification for Battery State-of-Charge Estimation. IEEE TRANSACTIONS ON INDUSTRIAL ELECTRONICS. 2022; 69(4): 3743-3751.
[17] Wang YJ, Zhang CB, Chen ZH. On-line battery state-of-charge estimation based on an integrated estimator. Applied Energy. 2017; 185: 2026-2032.
[18] Wang L, Ma J, Zhao X, Li XB, Zhang K. Online estimation of state-of-charge inconsistency for lithium-ion battery based on SVSF-VBL. Journal of Energy Storage. 2023; 67: 107657.
[19] Chiang Y-H, Sean W-Y, Ke J-C. Online estimation of internal resistance and open-circuit voltage of lithium-ion batteries in electric vehicles. Journal of Power Sources. 2011; 196: 3921-3932.
[20] Wang DQ, Yang Y, Gu TY. A hierarchical adaptive extended Kalman filter algorithm for lithium-ion battery state of charge estimation. Journal of Energy Storage.

2023; 62: 106831.
[21] Lai X, Zheng YJ, Sun T. A comparative study of different equivalent circuit models for estimating state-of-charge of lithium-ion batteries. Electrochimica Acta. 2018; 259: 566-577.
[22] Tian JQ, Xu RL, Wang YJ, Chen ZH. Capacity attenuation mechanism modeling and health assessment of lithium-ion batteries. Energy. 2021; 221: 119682.
[23] Sui X, He S, Meng JH, Teodorescu R, Stroe D-I. Fuzzy Entropy-Based State of Health Estimation for Li-Ion Batteries. IEEE JOURNAL OF EMERGING AND SELECTED TOPICS IN POWER ELECTRONICS. 2021; 9(4): 5125-5137.
[24] Yang NK, Song ZY, Hofmann H, Sun J. Robust State of Health estimation of lithium-ion batteries using convolutional neural network and random forest. Journal of Energy Storage. 2022; 48: 103857.
[25] Tang XP, Zhou YQ, Gao FR, Lai X. Joint estimation of state-of-charge and state-of-health for all cells in the battery pack using ‘‘leader-follower’’ strategy. 2023; 15: 100213.
[26] Jiang N, Pang H. Study on Co-Estimation of SoC and SoH for Second-Use Lithium-Ion Power Batteries. Electronics. 2022; 11: 1789.
[27] Xu YZ, Hu BH, Wu TZ, Xiao TY. Joint estimation of state of charge and state of health of lithium-ion battery based on fractional order model. Journal of Power Electronics. 2022; 22: 318-330.
[28] Hu PP, Tang WF, Li HC, Mark SL, Li CY, Lee CC. Joint State of Charge (SOC) and State of Health (SOH) Estimation for Lithium-Ion Batteries Packs of Electric Vehicles Based on NSSR-LSTM Neural Network. Energies. 2023; 16: 5313.
[29] Yu QQ, Huang YK, Tang AH, Wang C, Shen WX. OCV-SOC-Temperature Relationship Construction and State of Charge Estimation for a Series–Parallel Lithium-Ion Battery Pack. IEEE TRANSACTIONS ON INTELLIGENT TRANSPORTATION SYSTEMS. 2023; 24(6): 6362-6371.
[30] Park S, Kim J, Cho I. Hybrid SOC and SOH estimation method with improved noise immunity and computational efficiency in hybrid railroad propulsion system. Journal of Energy Storage. 2023; 72: 108385.
[31] Xu C, Zhang E, Jiang K, Wang KL. Dual fuzzy-based adaptive extended Kalman filter for state of charge estimation of liquid metal battery. Applied Energy. 2022; 327: 1020091.
[32] Biaz V, Moreira AC, Pinto JL, Nascimento M, Marques C. A particle filter-based virtual sensor for estimating the state of charge and internal temperature of lithium-ion batteries: Implementation in a simulated study case. Journal of Energy Storage. 2023; 61: 106814.
[33] Zhong L, Zhang CB, He Y, Chen ZH. A method for the estimation of the battery pack state of charge based on in-pack cells uniformity analysis. Applied Energy. 2014; 113: 558-564.
[34] Chen Y, Li RB, Sun ZY, Zhao L, Guo XG. SOC estimation of retired lithium-ion batteries for electric vehicle with improved particle filter by H-infinity filter. Energy Reports. 2023; 9: 1937-1947.
[35] Hao XY, Wang SL, Fan YC, Xie YX, Fernandez C. An improved forgetting factor

recursive least square and unscented particle filtering algorithm for accurate lithium-ion battery state of charge estimation. Journal of Energy Storage. 2023; 59: 106478.
[36] Zhang X, Wang YJ, Liu C, Cheng ZH. A novel approach of battery pack state of health estimation using artificial intelligence optimization algorithm. Journal of Power Sources. 2018; 376: 191-199.
[37] Shi E, Xia F, Peng DG, Li L, Wang XK, Yu BL. State-of-health estimation for lithium battery in electric vehicles based on improved unscented particle filter. Journal of Renewable and Sustainable Energy. 2019; 11: 02401.
[38] Dong GZ, Chen ZH, Wei JW, Ling Q. Battery Health Prognosis Using Brownian Motion Modeling and Particle Filtering. IEEE TRANSACTIONS ON INDUSTRIAL ELECTRONICS. 2018; 65(11): 8646-8655.
[39] Xu YH, Chen X, Zhang HG, Yang FB, Tong L, Yang YF, Yan D, Yang AR, Yu MZ, Liu ZX, Wang Y. Online identification of battery model parameters and joint state of charge and state of health estimation using dual particle filter algorithms. International Journal of Energy Research. 2022; 46: 19615-19652.
[40] Ghorbani N, Kasaeian A, Toopshekan A, Bahrami L. Optimizing a hybrid wind-PV-battery system using GA-PSO and MOPSO for reducing cost and increasing reliability. Energy. 2018; 154: 581-591.
[41] Mao XJ, Song SJ, Ding F. Optimal BP neural network algorithm for state of charge estimation of lithium-ion battery using PSO with Levy flight. Journal of Energy Storage. 2022; 49: 104139.
[42] Zheng YJ, Gao WK, Ouyang MG, Lu LG, Zhou L, Han XB. State-of-charge inconsistency estimation of lithium-ion battery pack using mean-difference model and extended Kalman filter. Journal of Power Sources. 2018; 383: 50-58.
[43] Feng F, Song B, Xu JN, Na W, Zhang K, Chai Y. Multiple time scale state-of-charge and capacity-based equalisation strategy for lithium-ion battery pack with passive equalizer. Journal of Energy Storage. 2022;53: 105196.
[44] Ouyang Q, Chen J, Zheng J, Hong YG. SOC Estimation-Based Quasi-Sliding Mode Control for Cell Balancing in Lithium-Ion Battery Packs. IEEE TRANSACTIONS ON INDUSTRIAL ELECTRONICS. 2018; 65(4):3427-346.
[45] Jing B, Dai HF, Wei XZ. A Cell-to-Pack State Estimation Extension Method Based on a Multilayer Difference Model for Series-Connected Battery Packs. IEEE TRANSACTIONS ON TRANSPORTATION ELECTRIFICATION. 2022; 8(2): 2037-2049.
[46] Shukla A, Singh SN. Advanced three-stage pseudo-inspired weight-improved crazy particle swarm optimization for unit commitment problem. Energy. 2016; 96: 23-36.
[47] Li HH, Qu ZW, Xu T, Wang YP, Fan XS, Jiang HB, Yuan CC, Chen L. SOC estimation based on the gas-liquid dynamics model using particle filter algorithm. International Journal of Energy Research. 2022; 46: 22913-22925.